ELSEVIER

Scopus

doi

Journal of Vibration Engineering

ISSN:1004-4523

Registered

- SCOPUS
- GOOGLE SCHOLAR
- DIGITAL OBJECT IDENTIFIER (DOI)
- IMPACT FACTOR 6.1

Our Website
www.jove.science

Analysis of Shape Effects on Heat and Mass Transformation in MHD Couple-Stress Squeezing Flow

Swetha Boppani[1], V Sridhar[1,*] and Adigoppula Raju[2]

[1]Department of Mathematics, Malla Reddy University, Telangana, India
[2]Dept. of Applied Sciences, Symbiosis Institute of Technology, Symbiosis International (Deemed University), Pune, India.

ABSTRACT:

The investigation of bioconvective hybrid nanofluid flow has garnered considerable interest owing to its extensive applications in biofuel production, biosensors, and biomedical engineering. The present work analyze the impact of non-spherical nanoparticle geometries on heat transfer and mass transport in the squeezing flow of magnetohydrodynamic couple stress hybrid nanofluid between parallel plates containing microorganisms. The governing nonlinear ordinary differential equations are solved numerically using the shooting method combined with the fourth-order Runge–Kutta scheme. The influence of key physical parameters is examined on velocity components, temperature, and microorganism density profiles. Furthermore, the skin friction coefficient, Nusselt number, and Sherwood number are computed for various dimensionless parameters. The obtained results demonstrate good agreement with previously published studies.

Keywords: hybrid nanofluid, shape effect, squeezing channel, couple stress, microorganisms, magnetohydrodynamic, shooting method.

Nomenclature:

$\mathbf{U,V}$:	Velocity components in [x, y] coordinates [ms^{-1}]
p :	Pressure [kg ms^{-2}]
η_1 :	Couple-stress viscous coefficient [N m^2]
σ:	Fluid Electrical conductivity [$s\ m^{-1}$]
μ :	Dynamic viscosity of fluid [kg $s^{-1}m^{-1}$]

ρ : Density of fluid [kg m^{-3}]

C : Concentration [kg m^{-3}]

D: Mass diffusivity [$m^2\ s^{-1}$]

D_m : Microorganism diffusivity [$m^2\ s^{-1}$]

N : Density of the microorganism [kg m^{-3}]

b_c : Chemotaxis Constant

ω_c : Maximum cell swimming speed

T : Temperature [k]

J: Current density [Am^{-2}]

$\bar{B}$: Applied magnetic field [T]

$\bar{E}$: Applied electric field [V m^{-1}]

ϕ_{MoS_2} : MoS_2 volume concentration

$\phi_{Al_2O_3}$: Al_2O_3 volume concentration

k : Thermal conductivity of fluid [$Wm^{-1}K^{-1}$]

C_p : Specific heat capacity [J $kg^{-1}K^{-1}$]

$\mathbf{C}_1$: Concentration at the bottom plate [kg m^{-3}]

$\mathbf{C}_2$: Concentration at the upper plate [kg m^{-3}]

$\mathbf{T}_R$: Wall temperature [K]

$\mathbf{C}_R$: Concentration of the top plate [kg m^{-3}]

$\mathbf{N}_R$: microorganisms density of the top plate [kg m^{-3}]

m: Sahpe factor $\{ m = \frac{3}{\varpi} \}$

ϖ : nanoparticle sphericity

$\mathbf{A_1}$, $\mathbf{A_2}$: various nanoparticle geometries coefficients (Table-2)

Non-dimensional numbers:

β: Couple stress parameter $\left\{\left(\frac{\eta_1}{h^2\mu_f}\right)^{0.5}\right\}$

Pr: Prandtl number $\left\{\frac{\mu_f\left(\rho C_p\right)_f}{\rho_f k_f}\right\}$

Ec: Eckert number $\left\{\frac{\rho_f}{(\rho C_p)_f \mathrm{T}_R}\left(\frac{\mathrm{a}x}{2(1-\mathrm{a}t)}\right)^2\right\}$

S: Squeezing parameter $\left\{\frac{\rho_f \mathrm{a}H^2}{2\mu_f}\right\}$

Ha: Hartman number of nanofluid $\left\{B_0 H\sqrt{(1-\mathrm{a}t)\frac{\sigma_f}{\mu_f}}\right\}$

Sc : Concentration Schmidt number $\left\{\frac{\mu_f}{\rho_f \mathrm{D}}\right\}$

Sc_m : Bioconvection Schmidt number $\left\{\frac{\mu_f}{\rho_f \mathrm{D}_m}\right\}$

Pe: Bioconvection Peclet number $\left\{\frac{b_c \omega_c}{\mathrm{D}_m}\right\}$

δ: Non-dimensional axial variable $\left\{\frac{H\sqrt{(1-\mathrm{a}t)}}{x}\right\}$

δ_c : Slip parameters in concentration $\left\{\frac{\mathrm{C}_R}{\mathrm{C}_1-\mathrm{C}_2}\right\}$

Subscripts:

f : Base Fluid

nf : Nanofluid

hnf : Hybrid nanofluid

MoS_2: Molybdenum disulphide

Al_2O_3: Aluminium oxide

1. INTRODUCTION

Heat transfer in squeezing flow between parallel plates has gained considerable attention because of its broad applications in lubrication devices, transmission of power, polymer synthesis, cooling technologies, and biomedical devices. The concept of squeezing flow was first introduced by Josef Stefan [1]. Later, Gupta et al. [2] examined unsteady flow between symmetrically approaching plates using the Navier–Stokes equations. Subsequent studies employed various analytical and numerical techniques to investigate similar unsteady flow problems by M. Sheikholeslami et al. [3], and R.C. Mittal et al. [4]. In recent years, researchers have extended these analyses to include heat and mass transfer effects under additional physical influences such as magnetohydrodynamics and slip boundary conditions by Mustafa et al. [5], M.G. Sobamowo [6], Kashyap et al. [7], Saif et al. [8]. Furthermore, the thermophysical characteristics of hybrid nanofluids, such as $CuO–Al_2O_3$/water flowing between parallel plates, has also been examined, with particular attention to variable viscosity effects Famakinwa et al. [9].

Various fluid flow models have been extensively studied, among which couple-stress fluids play a significant role in accurately describing physiological and industrial suspensions due to their ability to incorporate microrotation and size-dependent stress effects. Unlike Newtonian fluids, this theory accounts for microstructural behaviour and was originally introduced by George Gabriel Stokes [10]. Later, laminar incompressible couple-stress flow in expanding and contracting permeable channels was analysed by Srinivasacharya et al. [11], and heat transfer between immiscible fluid layers under magnetic influence was examined by Murthy and Srinivas [12]. Further investigations addressed micropolar and MHD couple-stress nanofluid flows, including the impact of Brownian motion and thermophoresis, investigated

by Raju et al. [13], Hayat et al. [14]. Time-dependent pressure variations Ilani et al. [15], thermal radiation effects studied by Raju et al. [16], and convective heat transfer through anisotropic porous media investigated by Bhargavi et al. [17] have also been explored, highlighting the broad applicability of couple-stress fluid models.

Nanoparticle geometry plays a crucial role in determining the thermal performance of nanofluids, as particle size, shape, and volume concentration significantly influence effective thermal conductivity and viscosity. Early theoretical studies by R. L. Hamilton and O. K. Crosser [18] showed that thermal conductivity significantly depends on particle shape. Experimental findings confirmed that surface characteristics markedly affect nanofluid viscosity, as reported by Timofeeva et al. [19]. Subsequent studies have examined various nanoparticle configurations under different physical conditions, including MHD mixed convection with Molybdenum disulfide in water, which was examined by Khan [20]. After that experimentally analysed the mixed convective flow with porous medium under a magnetic field by Ali Abro [21], MoS_2 nanoparticles dispersed in ethylene glycol (EG) showed enhanced thermal performance, as reported by Preeti et al. [22], as well as for GO–MoS_2 hybrid nanofluids under MHD flow conditions, Ghadikolaei and Gholinia [23]. Further investigations highlighted the influence of particle form factor on convective mass and heat transfer, as examined by Ananth Subray et al. [24], with platelet and blade-shaped nanoparticles demonstrating superior heat transfer improvement compared to other shapes, as explored by S. Li, X. You et al. [25] and Ahsan et al. [26], respectively. Additionally, the effect of nanoparticle type and shape on nanolubrication and three-dimensional MHD hybrid nanofluid flows has been explored, confirming that optimised geometries significantly improve thermal transport characteristics Imran et al. [27], Arif et al. [28].

Bioconvection has significant applications in biotechnology and biological transport processes, particularly in systems involving motile microorganisms. The concept of gravitate bioconvection for geotactic microorganisms was first introduced by Stephen Childress [29]. Since then, several studies have investigated bioconvective Nano liquid flow between parallel plates, incorporating the influence of microorganisms along with additional physical factors such as chemical reactions and magnetic fields using various numerical techniques by Bin-Mohsin et al. [30], Zhao et al. [31], Shamshuddin et al. [32], and Srinivasacharya and Sreenath [33, 34] More recently, research has extended to MHD couple-stress hybrid nanofluids to analyse their thermal and mass transfer characteristics by Raju et al. [35] and Samal et al. [36, 37], while entropy generation analysis in hybrid nanofluids has also been examined to evaluate system irreversibility and thermal efficiency, as examined by Thabet et al. [38].

To the best of current knowledge, the effect of non-spherical nanoparticles on bioconvective hybrid nanofluids with microorganisms has not yet been explored. This study, therefore, examines how particle shape influences heat and microorganism transport behaviour. The governing equations are reduced using similarity transformations and numerically solved via the shooting method with a fourth-order Runge–Kutta scheme. The variations in velocity, temperature, and microorganism profiles under different parameters are presented graphically.

2. PHYSICAL AND MATHEMATICAL DESCRIPTION

The present model investigates heat and mass transfer in a bioconvective hybrid nanofluid containing various shapes of MoS_2 and Al_2O_3 nanoparticles dispersed in water, flowing between two parallel plates under squeezing conditions in the presence of microorganisms. A two-dimensional, laminar, incompressible, unsteady, and electrically conducting flow

configuration is considered. The lower plate is at y = 0, while the upper plate is at y = h(t) at a distance $h(t) = H(1-\eta t)^{0.5}$, with the upper plate sliding closer to or farther away from the lower plate, depending on the squeezing parameter. The physical model framework is clearly illustrated in Fig. 1. The magnetic field is induced perpendicular to the flow direction $B(t) = B_o(1-\eta t)^{-0.5}$. The analysis incorporates distinct nanoparticle geometries—brick, cylinder, platelet, and blade shapes—to evaluate shape-dependent thermal behaviour. Additionally, a homogeneous magnetic field is induced perpendicular to the flow to examine magnetohydrodynamic effects on the system.

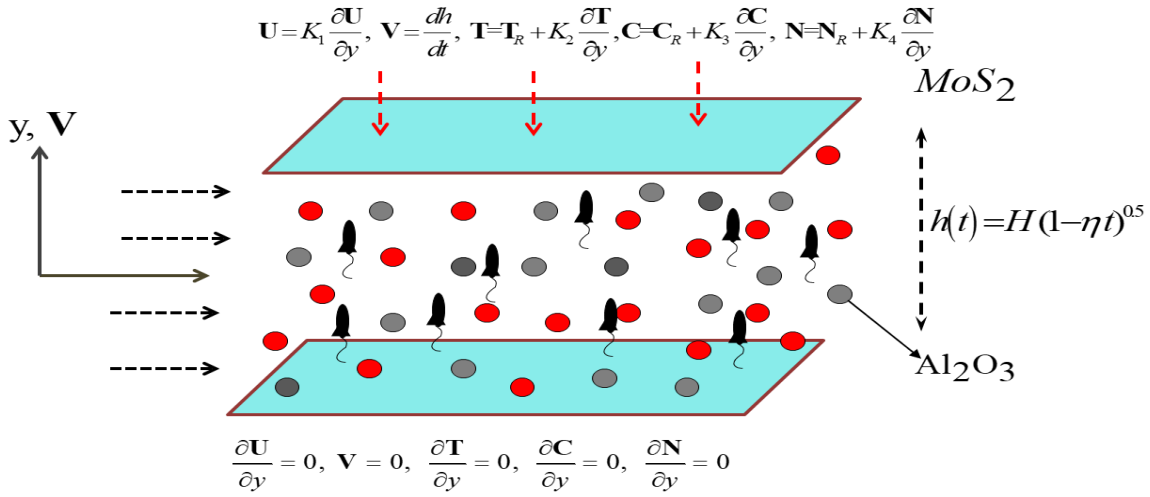

Fig. 1. Schematic Representation of the Physical Mode.

The following dimensional governing equations are formulated based on the methodology [5, 14, 35]

$$\frac{\partial \mathbf{U}}{\partial x} + \frac{\partial \mathbf{V}}{\partial y} = 0 \tag{1}$$

$$\rho_{hnf}\left(\frac{\partial \mathbf{U}}{\partial t} + \mathbf{U}\frac{\partial \mathbf{U}}{\partial x} + \mathbf{V}\frac{\partial \mathbf{U}}{\partial y}\right) = -\frac{\partial p}{\partial x} + \mu_{hnf}\left(\frac{\partial^2 \mathbf{U}}{\partial x^2} + \frac{\partial^2 \mathbf{U}}{\partial y^2}\right) - \eta_1\left(\frac{\partial^4 \mathbf{U}}{\partial x^4} + 2\frac{\partial^4 \mathbf{U}}{\partial x^2 \partial y^2} + \frac{\partial^4 \mathbf{U}}{\partial y^4}\right) - \sigma_{hnf} B^2 \mathbf{U} \tag{2}$$

$$\rho_{hnf}\left(\frac{\partial \mathbf{V}}{\partial t} + \mathbf{U}\frac{\partial \mathbf{V}}{\partial x} + \mathbf{V}\frac{\partial \mathbf{V}}{\partial y}\right) = -\frac{\partial p}{\partial y} + \mu_{hnf}\left(\frac{\partial^2 \mathbf{V}}{\partial x^2} + \frac{\partial^2 \mathbf{V}}{\partial y^2}\right) - \eta_1\left(\frac{\partial^4 \mathbf{V}}{\partial x^4} + 2\frac{\partial^4 \mathbf{V}}{\partial x^2 \partial y^2} + \frac{\partial^4 \mathbf{V}}{\partial y^4}\right) - \sigma_{hnf} B^2 \mathbf{V} \tag{3}$$

$$\left(\rho C_p\right)_{hnf}\left(\frac{\partial \mathbf{T}}{\partial t}+\mathbf{U}\frac{\partial \mathbf{T}}{\partial x}+\mathbf{V}\frac{\partial \mathbf{T}}{\partial y}\right)=k_{hnf}\left(\frac{\partial^2 \mathbf{T}}{\partial x^2}+\frac{\partial^2 \mathbf{T}}{\partial y^2}\right)+\mu_{hnf}\left[2\left(\frac{\partial \mathbf{U}}{\partial x}\right)^2+2\left(\frac{\partial \mathbf{V}}{\partial y}\right)^2+\left(\frac{\partial \mathbf{U}}{\partial y}+\frac{\partial \mathbf{V}}{\partial x}\right)^2\right]+\eta_1\left[\left(\frac{\partial^2 \mathbf{U}}{\partial x^2}+\frac{\partial^2 \mathbf{U}}{\partial y^2}\right)^2+\left(\frac{\partial^2 \mathbf{V}}{\partial x^2}+\frac{\partial^2 \mathbf{V}}{\partial y^2}\right)^2\right]+\sigma_{hnf}B_0^2\left(\mathbf{U}^2+\mathbf{V}^2\right) \tag{4}$$

$$\left(\frac{\partial \mathbf{C}}{\partial t}+\mathbf{U}\frac{\partial \mathbf{C}}{\partial x}+\mathbf{V}\frac{\partial \mathbf{C}}{\partial y}\right)=\mathrm{D}\left(\frac{\partial^2 \mathbf{C}}{\partial x^2}+\frac{\partial^2 \mathbf{C}}{\partial y^2}\right) \tag{5}$$

$$\frac{\partial \mathbf{N}}{\partial t}+\mathbf{U}\frac{\partial \mathbf{N}}{\partial x}+\mathbf{V}\frac{\partial \mathbf{N}}{\partial y}+\frac{b_c\omega_c}{\mathbf{C}_1-\mathbf{C}_2}\left[\frac{\partial}{\partial x}\left(\mathbf{N}\frac{\partial \mathbf{C}}{\partial y}\right)+\frac{\partial}{\partial y}\left(\mathbf{N}\frac{\partial \mathbf{C}}{\partial y}\right)\right]=\mathrm{D}_m\left(\frac{\partial^2 \mathbf{N}}{\partial x^2}+\frac{\partial^2 \mathbf{N}}{\partial y^2}\right) \tag{6}$$

Neglecting the displacement current, the governing forms of Ohm's law and Maxwell's equations can be written as follows.

$$\nabla\times\bar{E}=\frac{\partial \bar{B}}{\partial t},\ \nabla\times\bar{\mathbf{B}}=\mu_e\bar{J},\ \nabla.\bar{\mathbf{B}}=0,\ \bar{J}=\sigma(\bar{E}+\bar{q}\times\bar{\mathbf{B}}) \tag{7}$$

The flow boundary conditions assumed for the problem [7] are

$$\left.\begin{aligned} &at\ \mathrm{y}=0:- && \frac{\partial \mathbf{U}}{\partial y}=0,\ \mathbf{V}=0,\ \frac{\partial \mathbf{T}}{\partial y}=0,\ \frac{\partial \mathbf{C}}{\partial y}=0,\ \frac{\partial \mathbf{N}}{\partial y}=0\\ &at\ \mathrm{y}=\mathrm{h(t)}:- && \mathbf{U}=\mathrm{k}_1\frac{\partial \omega_1}{\partial y},\ \mathbf{V}=\frac{dh}{dt},\ \mathbf{T}=\mathbf{T}_R+\mathrm{k}_2\frac{\partial \mathbf{T}}{\partial y},\\ & && \mathbf{C}=\mathbf{C}_R+\mathrm{k}_3\frac{\partial \mathbf{C}}{\partial y},\ \mathbf{N}=\mathbf{N}_R+\mathrm{k}_4\frac{\partial \mathbf{N}}{\partial y} \end{aligned}\right\} \tag{8}$$

Where $\mathrm{k}_1,\mathrm{k}_2,\mathrm{k}_3,\ \mathrm{k}_4$ are slip constants

Table-1:- Hybrid nanofluid Thermo-physical correlations [18, 23-27]

Properties	Hybrid nanofluid
Density	$\rho_{hnf}=\left(1-\phi_{Al_2O_3}\right)\left[\left(1-\phi_{MoS_2}\right)\rho_f+\phi_{MoS_2}\rho_{MoS_2}\right]+\phi_{Al_2O_3}\ \rho_{Al_2O_3}$
Viscosity	$\mu_{hnf}=\mu_f\left(1+\mathbf{A_1}\phi+\mathbf{A_2}\phi^2\right)$ (Non Spherical) $\left(\phi=\phi_{MoS_2}+\phi_{Al_2O_3}\right)$
Heat Capacity	$\left(\rho\ C_p\right)_{nf}=\left(1-\phi_{Al_2O_3}\right)\left\{\left(1-\phi_{MoS_2}\right)\left(\rho\ C_p\right)_f+\phi_{MoS_2}\left(\rho\ C_p\right)_{MoS_2}\right\}+\phi_{Al_2O_3}\ \left(\rho\ C_p\right)_{Al_2O_3}$
	$\sigma_{hnf}=\sigma_{nf}\left[1+\frac{3\phi_{MoS_2}\left(\phi_{MoS_2}\sigma_{MoS_2}+\phi_{Al_2O_3}\sigma_{Al_2O_3}-\sigma_{nf}\left(\phi_{MoS_2}+\phi_{Al_2O_3}\right)\right)}{\left(\phi_{MoS_2}\sigma_{MoS_2}+\phi_{Al_2O_3}\sigma_{Al_2O_3}+2\phi_{MoS_2}\sigma_{nf}\right)-\phi_{MoS_2}\sigma_{nf}\left(\phi_{MoS_2}\sigma_{MoS_2}+\phi_{Al_2O_3}\sigma_{Al_2O_3}\right)-\sigma_{nf}\left(\phi_{MoS_2}+\phi_{Al_2O_3}\right)}\right]$

Electrical conductivity	Where $\sigma_{nf} = \sigma_f \left[1 + \frac{3\left(\sigma_{MoS_2} - \sigma_f\right)\phi_{MoS_2}}{\left(\sigma_{MoS_2} + 2\sigma_f\right) - \left(\sigma_{MoS_2} - \sigma_f\right)\phi_{MoS_2}} \right]$
Thermal Conductivity	$k_{hnf} = k_{nf} \left[\frac{k_{Al_2O_3} + (\mathrm{m}-1)k_{nf} - (\mathrm{m}-1)\phi_{Al_2O_3}\left(k_{nf} - k_{Al_2O_3}\right)}{k_{Al_2O_3} + (\mathrm{m}-1)k_{nf} + \phi_{Al_2O_3}\left(k_{nf} - k_{Al_2O_3}\right)} \right]$ Where $k_{nf} = k_f \left[\frac{k_{MoS_2} + (m-1)k_f - (m-1)\phi_{MoS_2}(k_f - k_{MoS_2})}{k_{MoS_2} + (m-1)k_f + \phi_{MoS_2}(k_f - k_{MoS_2})} \right]$

Table-2: Experimentally determined viscosity enhancement coefficients for various nanoparticle morphologies. [25]

Nanoparticle shape	**Brick**	**Cylinder**	**Platelet**	**Blade**
$\mathbf{A_1}$	1.9	13.5	37.1	14.6
$\mathbf{A_2}$	471.4	904.4	612.6	123.3
ϖ	0.81	0.62	0.52	0.36
m	3.7	4.8	5.7	8.3

Table-3:- The base fluid and nanoparticles thermo-physical characteristics [22, 26, 36]

Thermo-Physical characteristics	**Nanoparticles**		**Base fluid**
	MoS_2	**Al_2O_3**	**Blood**
Density (ρ) $[k\,gm^{-3}]$	5060	3970	1063
Heat Capacity (C_p) $[J\,kg^{-1}\,K^{-1}]$	397.746	765	3594
Electrical conductivity (σ) $[S\,m^{-1}]$	2.09*10^(-4)	35*10^(-6)	1.33
Thermal Conductivity (K) $[W\,m^{-1}K^{-1}]$	34.5	40	0.492

The similarity transformations [5, 7, 35]

$$\left.\begin{aligned} &\varsigma = \frac{y}{\mathrm{H}(1\text{-}\eta \mathrm{t})^{0.5}},\ \mathbf{U} = \frac{\eta x}{2(1-\eta t)}\mathrm{f}'(\varsigma), \mathbf{V} = \frac{-\eta \mathrm{H}}{\mathrm{H}(1\text{-}\eta \mathrm{t})^{0.5}}\mathrm{f}(\varsigma), \\ &\Theta = \frac{\mathbf{T}}{\mathbf{T}_R},\ \ \Phi = \frac{\mathbf{C}}{\mathbf{C}_R},\ \ \Psi = \frac{\mathbf{N}}{\mathbf{N}_R} \end{aligned}\right\} \tag{9}$$

We derived the subsequent results by substituting Equation (9) into the preceding partial differential equations. (1) – (6).

$$\mathrm{f}'''' = \frac{1}{\beta^2}\left[\mathrm{E}_5\,\mathrm{f}'''' - \mathrm{E}_4 Ha^2\,\mathrm{f}'' - \mathrm{E}_1 S(\varsigma\,\mathrm{f}''' + 3\mathrm{f}'' + \mathrm{f}'\,\mathrm{f}'' - \mathrm{f}''')\right] \tag{10}$$

$$\Theta'' = \frac{\mathrm{Pr}}{\mathrm{E}_3}\left[\mathrm{E}_2 S(\varsigma - \mathrm{f})\Theta' - Ec\left\{\begin{aligned}&\mathrm{E}_5\left(4\delta^2(\mathrm{f}')^2 + (\mathrm{f}'')^2\right) + \beta^2\left((\mathrm{f}''')^2 + \delta^2(\mathrm{f}'')^2\right) + \\ &\mathrm{E}_4 Ha^2\left((\mathrm{f}')^2 + \delta^2\,\mathrm{f}^2\right)\end{aligned}\right\}\right] \tag{11}$$

$$\Phi'' = S\,Sc\left(\varsigma - \mathrm{f}\right)\Phi' \tag{12}$$

$$\Psi'' = S\,Sc_m\left(\varsigma - \mathrm{f}\right)\Psi' + Pe\,\delta_c\left(\Psi'\Phi' + \Psi\Phi''\right) \tag{13}$$

Here, velocity, temperature, concentration, and microorganism density are represented as unknown functions $\mathrm{f}(\varsigma), \Theta(\varsigma), \Phi(\varsigma), \Psi(\varsigma)$ respectively. While $\mathrm{E}_1, \mathrm{E}_2, \mathrm{E}_3, \mathrm{E}_4, \mathrm{E}_5$ are dimensionless parameters which are mentioned in equations. (14) – (18), and these are calculated by using Table-1 to 3 values. The prime symbol (′) shows that there is a difference in the similarity variable ς. By using the idea of [23, 27] mentioned below.

$$\mathrm{E}_1 = \frac{\rho_{hnf}}{\rho_f} = (1-\phi_{Al_2O_3})\left(1-\left(1-\frac{\rho_{MoS_2}}{\rho_f}\right)\phi_{MoS_2}\right) + \phi_{Al_2O_3}\frac{\rho_{Al_2O_3}}{\rho_f} \tag{14}$$

$$\mathrm{E}_2 = \frac{(\rho C_\mathrm{P})_{hnf}}{(\rho C_\mathrm{P})_f} = (1-\phi_{Al_2O_3})\left(1-\left(1-\frac{(\rho C_\mathrm{P})_{MoS_2}}{(\rho C_\mathrm{P})_{nf}}\right)\phi_{MoS_2}\right) + \phi_{Al_2O_3}\frac{(\rho C_\mathrm{P})_{Al_2O_3}}{(\rho C_\mathrm{P})_{nf}} \tag{15}$$

$$\mathrm{E}_3 = \frac{k_{hnf}}{k_f} = \frac{k_{Al_2O_3} + (\mathrm{m}-1)k_f - (\mathrm{m}-1)\phi_{Al_2O_3}(k_f - k_{Al_2O_3})}{k_{Al_2O_3} + (\mathrm{m}-1)k_f + \phi_{Al_2O_3}(k_f - k_{Al_2O_3})} \cdot \frac{k_{MoS_2} + (\mathrm{m}-1)k_f - (\mathrm{m}-1)\phi_{MoS_2}(k_f - k_{MoS_2})}{k_{MoS_2} + (\mathrm{m}-1)k_f + \phi_{MoS_2}(k_f - k_{MoS_2})} \tag{16}$$

$$E_4=\frac{\sigma_{hnf}}{\sigma_f}=\left[1+\frac{\left(3(m-1)\left(\frac{\sigma_{Al_2O_3}}{\sigma_f}-1\right)\phi_{Al_2O_3}\right)}{\left(\frac{\sigma_{Al_2O_3}}{\sigma_f}+2\right)-\left(\frac{\sigma_{Al_2O_3}}{\sigma_f}-1\right)(m-1)\phi_{Al_2O_3}}+\frac{\left(3(m-1)\left(\frac{\sigma_{MoS_2}}{\sigma_f}-1\right)\phi_{MoS_2}\right)}{\left(\frac{\sigma_{MoS_2}}{\sigma_f}+2\right)-\left(\frac{\sigma_{MoS_2}}{\sigma_f}-1\right)(m-1)\phi_{MoS_2}}\right] \quad (17)$$

$$E_5=\frac{\mu_{hnf}}{\mu_f}=\left(1+\mathbf{A}_1\phi+\mathbf{A}_2\phi^2\right) \quad (18)$$

The Arrived non-dimensional boundary condition Eq. (19) obtained by inserting Eq. (9) in Eq. (8) [7, 35]

$$\left.\begin{aligned} &at\ y=0\text{:-}\ \ f(y)=f'(y)=f''(y)=\Theta'(y)=\Phi'(y)=\Psi'(y)=0\\ &at\ y=1\text{:-}\ \ f(y)=1, f''(y)=0, f'(y)=U_s f''(y), \Theta(y)=1+T_s\Theta'(y)\\ &\qquad\qquad \Phi(y)=1+C_s\Phi'(y), \Psi(y)=1+N_s\Psi'(y)\end{aligned}\right\} \quad (19)$$

Here, U_s, T_s, C_s, and N_s quantities represent the dimensionless slip parameters associated with velocity, temperature, concentration, and microorganisms, respectively, and they depend on k_1, k_2, k_3, and k_4 parameters and accordingly [7].

$$U_s=\frac{k_1}{H(1-\eta t)^{0.5}}, T_s=\frac{k_2}{H(1-\eta t)^{0.5}}, C_s=\frac{k_3}{H(1-\eta t)^{0.5}}, N_s=\frac{k_4}{H(1-\eta t)^{0.5}} \quad (20)$$

The Skin friction (C_f), Nusselt (Nu_x) and Sherwood (Sh_x) numbers are measured at the top plate y = h(t) and the dimensionless forms are from Raju et al. [35]

$$\left.\begin{aligned} &C_f=\frac{\tau_w}{\rho_{nf}\upsilon_w^{\,2}};\quad Nu_x=\frac{Hq_w}{k_f T_R};\quad Sh_x=\frac{Hq_m}{DC_R}\\ &where\ \ \tau_w=\mu_{hnf}\left(\frac{\partial U}{\partial y}\right); q_w=-k_{hnf}\left(\frac{\partial T}{\partial y}\right); q_m=-D\left(\frac{\partial C}{\partial y}\right)\end{aligned}\right\} \quad (21)$$

$$\left.\begin{aligned} &C_f^*=\frac{x^2(1-\eta t)\mathrm{Re}_x C_f}{H^2}=\frac{f''(1)}{G_1\left(1-\phi_{MoS_2}\right)^{2.5}},\ where\ \mathrm{Re}_x=\eta H^5/2x^3(1-\eta t)^{1/2}\\ &Nu_x^*=\sqrt{1-\eta t}\,Nu_x=-E_3\Theta'(1),\ Sh_x^*=\sqrt{1-\eta t}\,Sh_x=-\Phi'(1)\end{aligned}\right\} \quad (22)$$

3. SOLUTION PROCEDURE USING NUMERICAL SCHEME

In the present work, the nonlinear ODE system defined in Eqs. (10–13) and (19) is solved numerically using the fourth-order Runge–Kutta (RK4) method combined with the shooting technique. The higher-order equations are first reduced to a system of first-order equations, and the boundary value problem (BVP) is converted into an initial value problem (IVP). The unknown initial conditions are determined using the Newton–Raphson method. The MATLAB implementation uses relative and absolute tolerances of 10^{-6}, ensuring stable, accurate convergence. The detailed computational steps are outlined below.

$$\left(\mathrm{f},\ \mathrm{f}',\mathrm{f}'',\ \mathrm{f}''',\ \mathrm{f}'''',\ \mathrm{f}''''\right)=\left(G_1,G_2,G_3,G_4,G_5\right) \tag{23}$$

$$\mathrm{f}''''=\frac{1}{\beta^2}\left(\mathrm{E}_5G_5-\mathrm{E}_4Ha^2G_3-\mathrm{E}_1S(\varsigma G_4+3G_3+G_2G_3-G_1G_4)\right) \tag{24}$$

$$\left(\Theta\ \ \Theta'\right)=\left(G_7\ \ \mathrm{G}_8\right) \tag{25}$$

$$\Theta''=\frac{\mathrm{Pr}}{\mathrm{E}_3}\left(\mathrm{E}_2S(\varsigma-G_1)\mathrm{G}_8-Ec\left\{\mathrm{E}_5\left(4\delta^2\,\mathrm{G}_2{}^2+\mathrm{G}_3{}^2\right)+\beta^2\left(\delta^2\,\mathrm{G}_3{}^2+\mathrm{G}_4{}^2\right)+\mathrm{E}_4Ha^2\left(\mathrm{G}_2{}^2+\delta^2G_1{}^2\right)\right\}\right) \tag{26}$$

$$\left(\Phi\ \ \Phi'\right)=\left(G_9\ \ \mathrm{G}_{10}\right) \tag{27}$$

$$\Phi''=S\,Sc\left(\varsigma-G_1\right)G_{10} \tag{28}$$

$$\left(\Psi\ \ \Psi'\right)=\left(G_{11}\ \ \mathrm{G}_{12}\right) \tag{29}$$

$$\Psi''=S\,Sc_m\left(\varsigma-G_1\right)G_{12}+Pe\ \delta_c\left(G_{12}G_{10}+G_{11}\Phi''\right) \tag{30}$$

4. RESULTS AND THEIR DISCUSSION

This study investigates the effects of key physical parameters on the axial and radial velocities, temperature, and microorganism density of a MoS_2-Al_2O_3/ Blood hybrid nanofluid containing non-spherical nanoparticles. The present analysis indicates that the proposed blood-based hybrid nanomaterials have promising biomedical applications, with MoS_2 used in cancer photothermal therapy, biosensing, medical imaging, and antibacterial treatments, while Al_2O_3 is applied in drug delivery, biosensing, and cancer therapy. The results demonstrate that the nanoparticle shape factor significantly influences both thermal and microbial distribution characteristics.

4.1 Effect of Physical Parameters on Axial Velocity

Fig. 2A—2C illustrate the axial velocity distributions of the MoS_2-Al_2O_3/ Blood hybrid nanofluid of the couple-stress, Hartmann number, and squeezer parameters with different nanoparticle geometries. Fig. 2A shows that the couple-stress parameter rises, reduces the axial velocity near the walls and the acceleration at the channel centre. This is because increased couple stress responses enhance microstructural resistance and rotational viscosity in the fluid, which inhibit the axial transport of all nanoparticle shapes. The opposite trend is observed: axial velocity increases towards the channel walls and decreases towards the channel centre with increasing Ha (Fig. 2B). This behaviour can be explained physically by the Lorentz force generated by the applied magnetic field, which opposes the fluid motion [29]. On the other hand, the brick shape factor causes nanoparticles to respond more slowly because they have a higher effective inertia and viscous drag, as shown in Figs. 2B. The velocity can also be given by the increasing parameter of squeezing as shown in Figs. 2C when the channel narrows the pressure gradient and shear forces become strong, the fluid movement becomes concentrated in the near-wall zone, and minimal in the core zone [32]. Most nanoparticle shapes have their velocities tightly concentrated, but platelet-like nanoparticles produce a somewhat higher flow structure due to their layered morphology, large surface area, thus, raise particle–particle interactions, hydrodynamic resistance, and viscous drag and, therefore, reduce flow mobility.

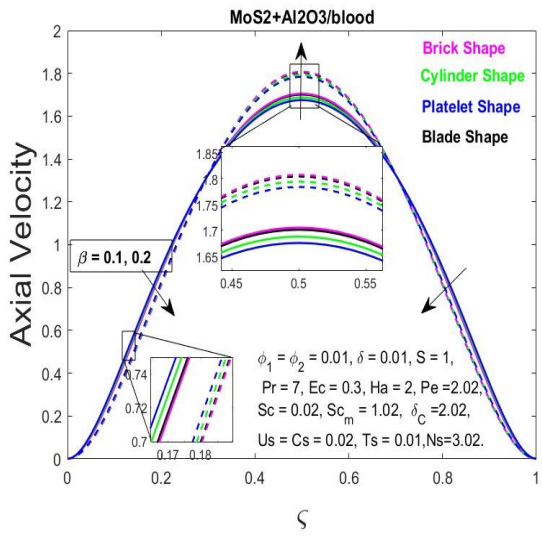

2A

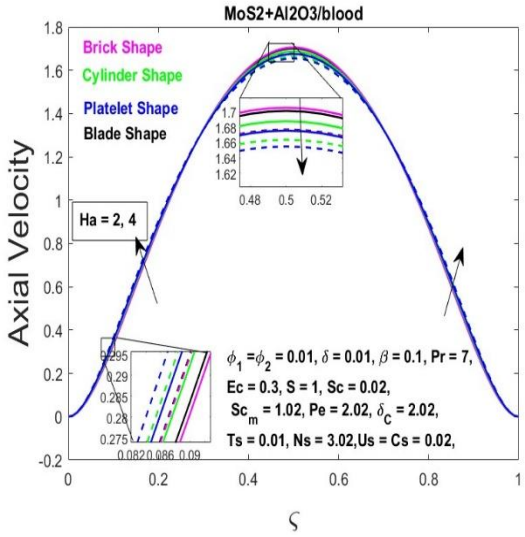

2B

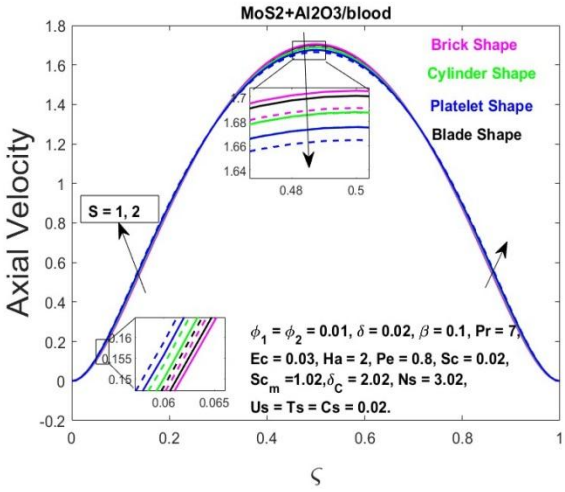

2(C)

Fig. 2A—2C: Axial Velocity Vs β, Ha, S

4.2. Effect of Physical Parameters on Radial Velocity

Fig. 3A—3C show the radial velocity distributions of the MoS_2-Al_2O_3/ Blood hybrid nanofluid under the effects of the couple-stress, Ha, and squeezer parameters of the different geometries of nanoparticles. Fig. 3A shows that the radial velocity diminishes towards the centre of the channel, then an increase is observed through the growth of β parameter of the shapes of nanoparticles. The reverse of this pattern is observed by Ha, and S. Fig. 3B illustrates the radial velocity to increase as the Hartmann number increases, and then

gradually decreases as a result of the Lorentz force and viscous resistance against radial movement [29] of all the shapes of nanoparticles. The same tendency is observed in the case of enhancement of the squeezing parameter of Fig. 3C, with channel walls squeezing the fluid in all shapes of nanoparticles. The platelet-shaped nanoparticles possess a low radial velocity due to the increased surface area and layered structure [28].

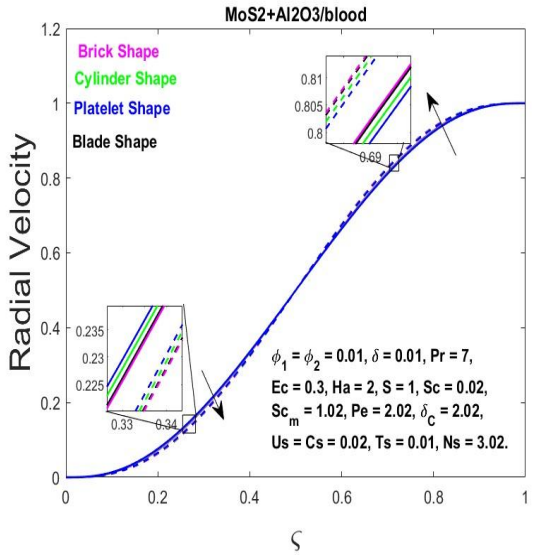

3A

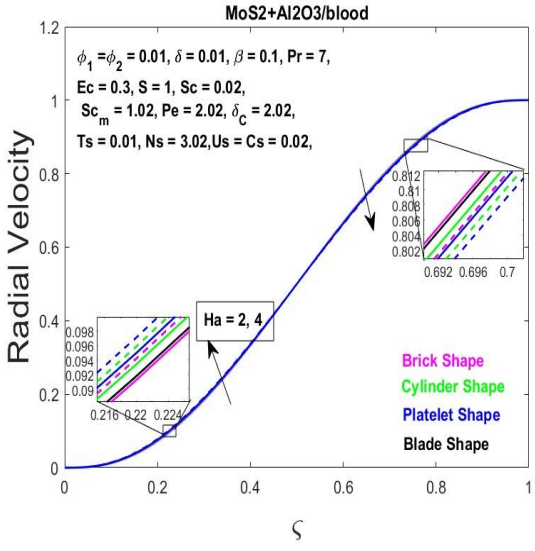

3B

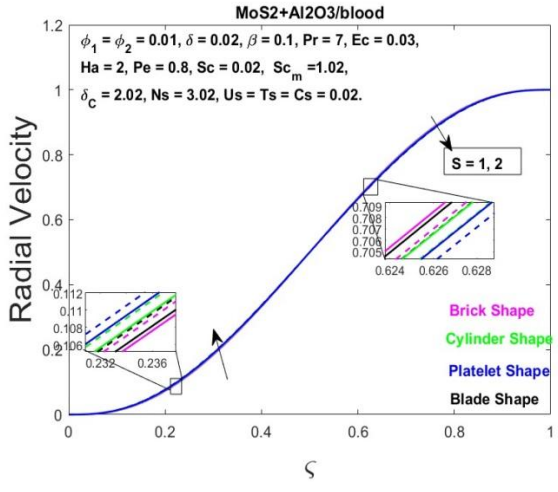

3C

Fig. 3A—3C: Radial velocity Vs β, Ha, S

4.3. Temperature Transport Characteristics

Fig. 4A—4G depict the significant alteration of the thermal properties of the MoS_2-Al_2O_3/ Blood hybrid nanofluid under the most significant governing parameters. All the evaluated parameters increase the temperature except the temperature slip parameter (Ts). A discernible trend in temperature profiles is seen among four nanofluids with varying geometries (brick > cylinder > platelet > blade). Where maximum temperature increment is exhibited by brick shape due to the existence of special geometry, high effective surface area, high thermal conductivity [28], high flow resistance, and high viscous dissipation when using brick-shaped nanoparticles. However, the former has a slight increase in viscosity as compared with the latter, and the latter has a slightly higher increase as compared to the former, due to the shape factor [28]. Fig. 4A indicates that as β parameter increases, the micro rotation effect increases, as a result, internal fluid friction increases, resulting in more heat being generated. According to Fig. 4B, the growth in the Hartmann number (Ha) prevents convective movement by the aid of magnetic damping and leads to heat enhancement in the channel [29]. As Fig. 4C shows, larger values of Pr boost the thermo-transport processes and this increases the value of the temperature field. Fig. 4D indicates that, as Eckert numbers (Ec) are increased, the temperature rises remarkably as the rate of viscous dissipation and the transformation of the kinetic energy into internal energy go up [25].According to Fig. 4E the temperature rises with the axial variable as a result of increasing thermal energy accumulation along the flow direction and longer contact of the fluid and the surface. The shapes of Fig. 4F show that the squeeze intensity enhances compression of the fluids and heating viscosity, which elevates the thermal field. On the other hand, Fig. 4G indicates the reverse since the greater the temperature slip parameter the lower the temperature of all shapes of nanoparticles with the lowest temperature recorded in the case of the brick-shaped nanoparticles due to low thermal interactions. These observations show that in addition to the influence of magnetism, the geometry of nanoparticles also matters to hybrid nanofluid flows.

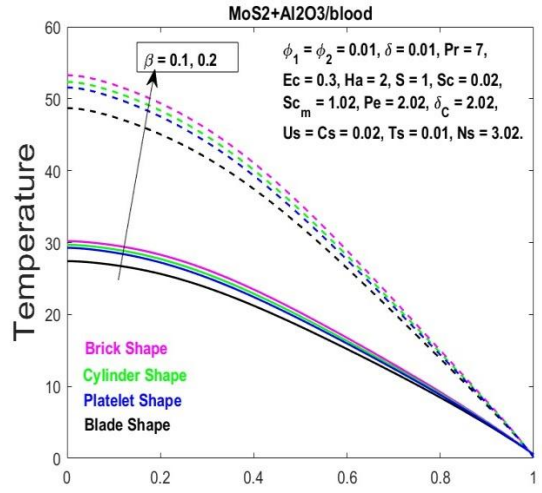

4A

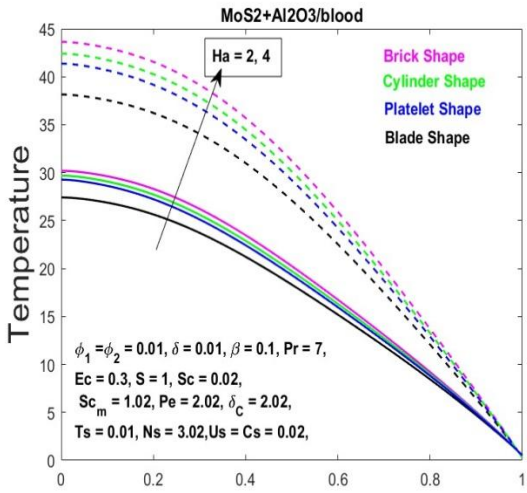

4B

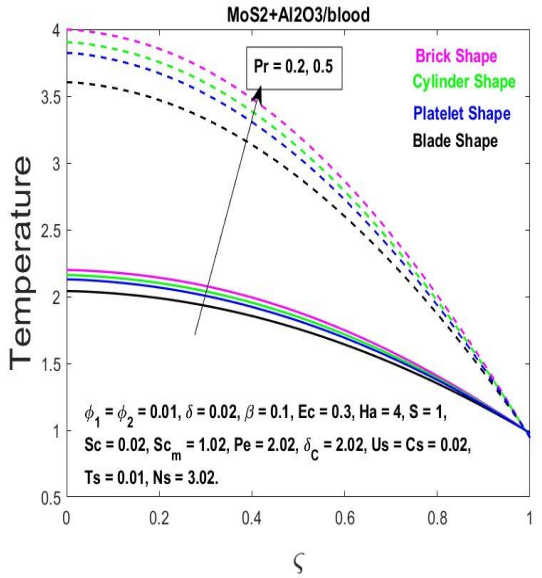

4C

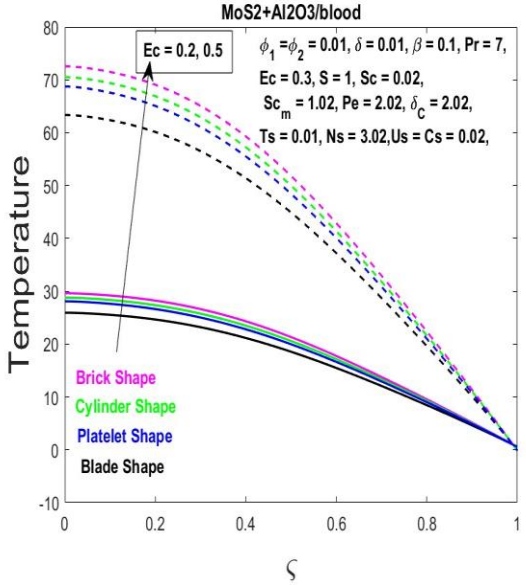

4D

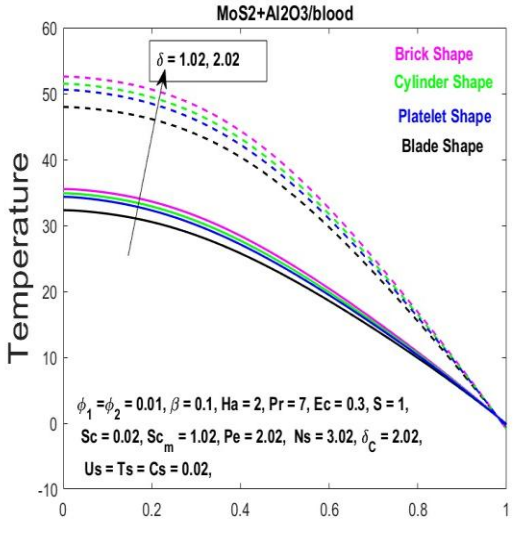

4E

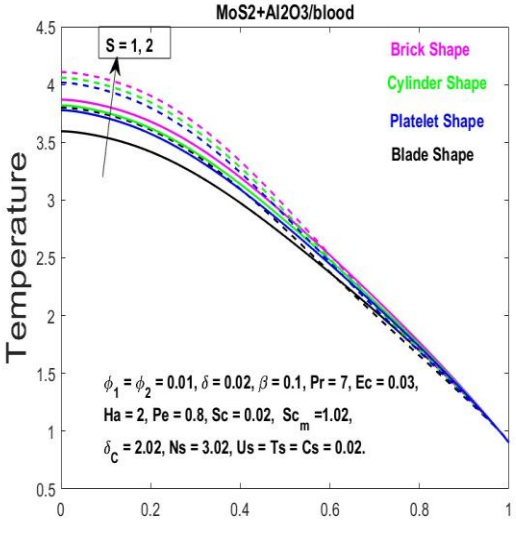

4F

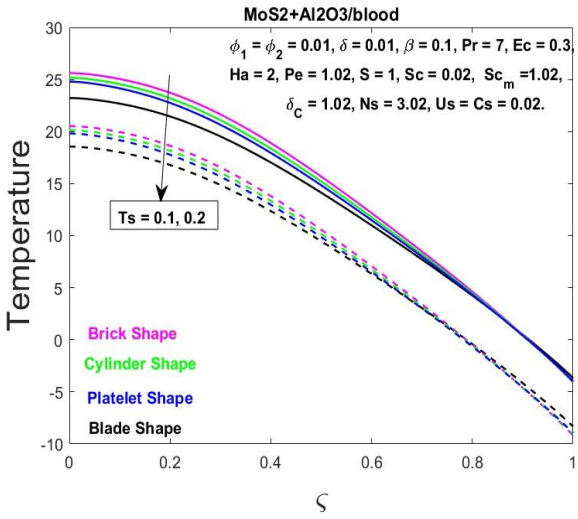

4G

Fig. 4A—4G: Temperature Vs β, Ha, Pr, Ec, δ_C ,S,Ts.

4.4. Microorganism density Behaviour

Fig. 5A—5H show that the distribution of microorganisms in the MoS_2-Al_2O_3/ Blood hybrid nanoliquid is dependent on the various parameters of flow with the nanoparticle shape factor being taken into account. The general results confirm that nanoparticles geometry plays a tremendous role in microorganism transportation. Fig. 5A shows that β parameter is enhanced, and this enhances the concentration of the microorganisms. The brick like nanoparticles increase its density due to its highest resistance to flow as compared to platelet like nanoparticles, which have the least response owing to their layered structure. The parameter S increases the concentration of the microorganism, as shown in Fig. 5B, due to compression of the fluid and enhances the near-wall concentration. Fig. 5C indicates that the more the concentration slip parameter, the higher the concentration of the microorganisms. In Fig. 5D, which indicates that the density of microorganisms is enhanced with rising Peclet number due to less diffusivity. Fig. 5E shows that when the microorganism slip parameter raises microorganisms density is enhanced. Fig. 5F shows that the improved Schmidt number leads to decreasing mass diffusivity, which causes a rise in concentration of the microorganisms with blade-shaped nanoparticles showing the highest response to the

geometry and platelet-shaped nanoparticles showing the least response to the increased drag and layered structure. On the other hand, Fig. 5G and 5H describe the reduction in the concentration of microorganisms as the Ha number and bioconvective Schmidt number increase due to the magnetic damping and the bioconvective motion inhibition. Platelet-shaped nanoparticles have the greatest falling response in the density of microorganisms of all other geometries, the brick-shaped nanoparticles have the lowest falling response by virtue of their shape factor.

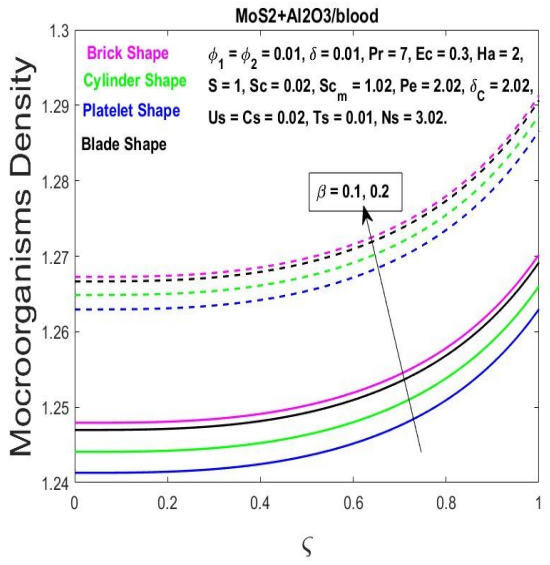

5A

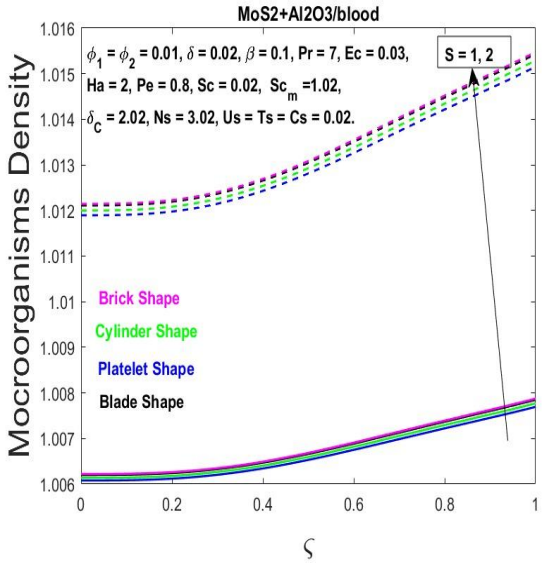

5B

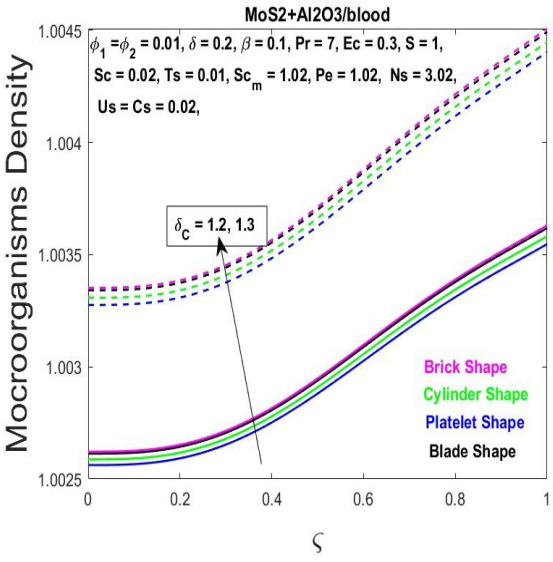

5C

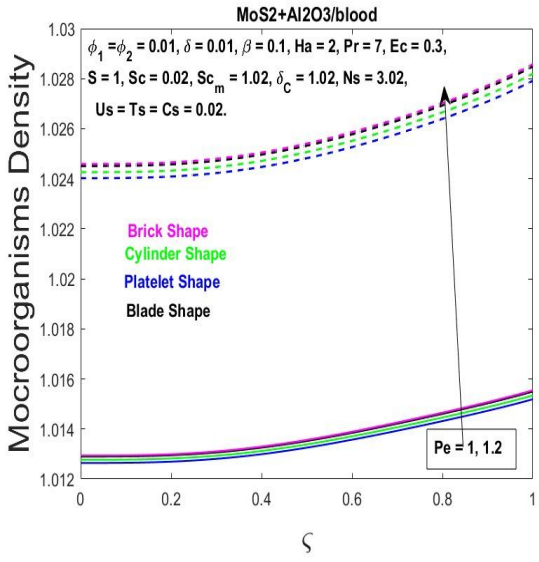

5D

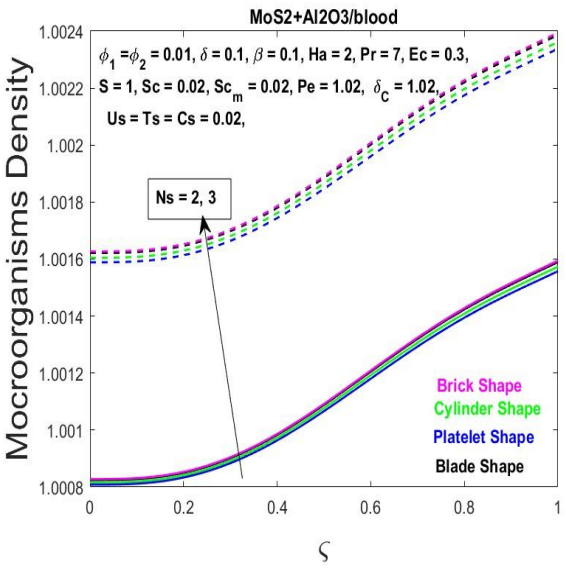

5E

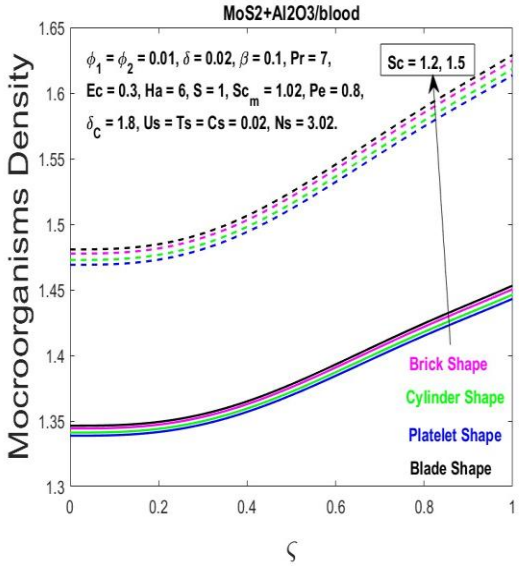

5F

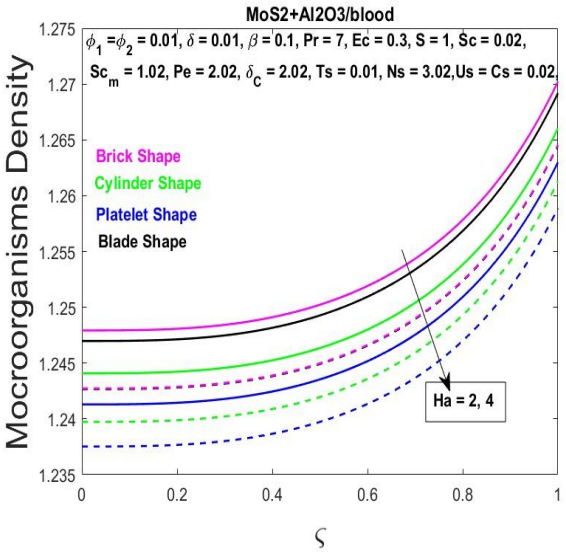

5G

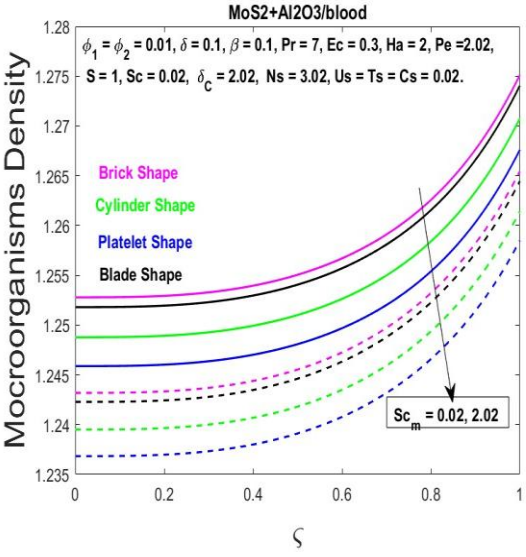

5H

Fig. 5A—5H: Microorganism Vs β, S, δ_C, Pe, Ns, Sc, Ha, Sc_m.

Table-4:- Skin-friction, Nusselt, Sherwood number values evaluated at S = 1, Ha = 2, $\phi_1 = \phi_2 = 0.01, \delta = 0.01, \beta = 0.1, \delta_C = 2.02$, Pr =7, Ec = 0.3, Sc =0.02, Sc_m = 1.02, Pe = 2.02, Ns = 3.02, and Us = Ts = Cs = 0.02.

	Nanoparticle Shapes	Squeezing parameter (S)		Couple stress parameter(β)		Hartmann number (Ha)		Bioconvective Schmidt number (Sc_m)	
		1	3	0.1	0.2	2	4	0.02	2.02
Skin-fricti	Blade	-0.9896	-1.0200	-0.9896	-0.7155	-0.9896	-1.0448	-0.9896	-0.9896
	Brick	-0.9715	-1.0027	-0.9715	-0.7082	-0.9715	-1.0373	-0.9715	-0.9715

	Cylinder	-1.0427	-1.0710	-1.0427	-0.7373	-1.0427	-1.1007	-1.0427	-1.0427
	Platelet	-1.0993	-1.1256	-1.0993	-0.7615	-1.0993	-1.1517	-1.0993	-1.0993
Nusselt number	Blade	44.9699	41.3938	44.9699	79.7325	44.9699	63.9295	44.9699	44.9699
	Brick	49.1879	44.8418	49.1879	86.3562	49.1879	72.6861	49.1879	49.1879
	Cylinder	48.3282	44.3718	48.3282	84.9052	48.3282	70.6601	48.3282	48.3282
	Platelet	47.5999	43.9293	47.5999	83.6880	47.5999	68.9020	47.5999	47.5999
Sherwood number	Blade	-1.0000	-1.0000	-1.0000	-1.0000	-1.0000	-1.0000	-1.0000	-1.0000
	Brick	-1.0000	-1.0000	-1.0000	-1.0000	-1.0000	-1.0000	-1.0000	-1.0000
	Cylinder	-1.0000	-1.0000	-1.0000	-1.0000	-1.0000	-1.0000	-1.0000	-1.0000
	Platelet	-1.0000	-1.0000	-1.0000	-1.0000	-1.0000	-1.0000	-1.0000	-1.0000

Table-4 indicates that the Sherwood number stays invariant at −1.0000, signifying that mass transfer is unaffected by the parameters under consideration. The Skin friction (C_f), Nusselt (Nu_x) numbers remain constant with a rise in the bioconvective Schmidt number (Sc_m). Both C_f and Nu_x numbers increase with an elevation in the couple stress parameter, however a contrary tendency is noted for elevated squeezing numbers. Moreover, C_f diminishes as the Nu_x number escalates with an increase in the Hartmann number. The nanoparticle shape follows the hierarchy: Brick > Blade > Cylinder > Platelet, showing increasing values in this order.

Table-5:- In the absence of microorganisms, the current results are validated with Mustafa et al. [5] by comparing the skin-friction coefficient for various values of S when Pr = Ec = Sc =1, Ha= β =0.

	HAM [5]	Present values
S = -1.0	2.17009	2.170090881
S = -0.5	2.614038	2.617403844
S = 0.01	3.007134	3.007133755
S = 0.5	3.336449	3.336449465
S = 2.0	4.167389	4.167389189

5. CONCLUSIONS

The paper investigates the effects of MoS_2, Al_2O_3 non-spherical (brick, cylindrical, platelet, and blade) shape nanoparticles on heat and mass transfer within a hybrid nanofluid consisting of blood between compressing parallel plates, taking into account the effects of couple-stress and magnetic field. Mathematical modelling is done in MATLAB with the help of the shooting method and the fourth-order Runge-Kutta scheme to solve the governing equations. The findings are useful in heat transfer enhancement in such systems as biomedical transport, microfluidic cooling, lubrication systems, and bio-thermal energy management. Genetic modification of microorganisms is beneficial in medicine, agriculture, cleaning the environment and industrial production.

- The hybrid nanofluid temperature rises with an increase in β, Ha, δ, Ec, Pr, and S.
- Among all the geometries of nanoparticles (brick, blade, cylinder, platelet), the brick-shaped particles exhibit the highest, and the blade-shaped particles exhibit the lowest thermal enhancement.
- The temperature of the hybrid nanofluid drops with an increase in the temperature slip parameter.
- The microorganisms' density increases with higher values of β, S, δ_C, Pe, N_S, Sc.
- The Ha and Sc_m increase leads to a decrease in the density of microorganisms.
- The platelet-shaped nanoparticles reduce microorganisms' density faster than other shapes.
- Skin-friction and Nusselt numbers increase with the couple stress parameter, whereas they decrease with higher squeezing numbers.
- The numerical findings are highly correlated with the available literature [5].

Future Work:

- The model can be applied to different base fluids like kerosene, Ethylene glycol, etc. and nanoparticles can be used like Cu, Ag, Zn, etc.
- The study can be extended to different nanoparticle shapes and sizes.
- The study can be extended by changing the geometry and different boundary conditions.
- The study can be further extended by including additional effects in the temperature and concentration equations, such as thermal radiation and heat generation/absorption.
- It can be useful for engineering applications.
- Experimental validation of the present numerical results can be carried out.

REFERENCES

1. M.J. Stefan, Versuche, uber die scheinbare adh¨asion, Akadenie deer Wissenschaften in Wien, Math.- Naturw 69 (1874) 713–721.
2. P. S. Gupta and A. S. Gupta, Squeezing flow between parallel plates, 45(2) (1977) 177–185, https://doi.org/10.1016/0043-1648(77)90072-2.
3. M. Sheikholeslami, D. D. Ganji, H. R. Ashorynejad, Investigation of squeezing unsteady nanofluid flow using ADM, Powder Technology 239 (2013) 259-265, https://doi.org/10.1016/j.powtec.2013.02.006.
4. R. C. Mittal, S. Pandit, Numerical simulation of unsteady squeezing nanofluid and heat flow between two parallel plates using wavelets, Int. J. Therm. Sci. 118 (2017) 410-422, https://doi.org/10.1016/j.ijthermalsci.2017.04.019.
5. M. Mustafa, T. Hayat, S. Obaidat, On heat and mass transfer in the unsteady squeezing flow between parallel plates, Meccanica, 47(7) (2012) 1581-1589, https://doi.org/10.1007/s11012-012-9536-3.

6. M. G. Sobamowo, A. T. Akinshilo, On the analysis of squeezing flow of nanofluid between two parallel plates under the influence of magnetic field, Alexandria Eng. J. 57(3) (2018) 1413-1423, https://doi.org/10.1016/j.aej.2017.07.001.
7. K. P. Kashyap, N. N. Kumar, Squeezing flow of a chemically reacting upper convected Maxwell nanofluid with slip effects, J. Nanofluids. 8(3) (2019) 509-519, https://doi.org/10.1166/jon.2019.1605.
8. A. S. Al-Saif, A. Harfash, Perturbation-iteration algorithm for solving heat and mass transfer in the unsteady squeezing flow between parallel plates, J. App. Comput. Mech. 5(4) (2019) 804-815, https://doi.org/10.22055/jacm.2019.28052.1453.
9. O. A. Famakinwa, O. K. Koriko, K. S. Adegbie, Effects of viscous dissipation and thermal radiation on time dependent incompressible squeezing flow of CuO−Al2O3/water hybrid nanofluid between two parallel plates with variable viscosity, J. Comput. Math. Data Sci. 5 (2022) 100062, https://doi.org/10.1016/j.jcmds.2022.100062.
10. V. K. Stokes, Couple stresses in fluids, In Theories of fluids with microstructure: an introduction Berlin, Heidelberg: Springer Berlin Heidelberg, (1984) 34-80, https://doi.org/10.1007/978-3-642-82351-0_4.
11. D. Srinivasacharya, N. Srinivasacharyulu, O. Odelu, Flow and heat transfer of couple stress fluid in a porous channel with expanding and contracting walls, Int. Commu. heat mass Transfer. 36 (2) (2009) 180-185, https://doi.org/10.1016/j.icheatmasstransfer.2008.10.005.
12. J. R. Murthy, J. Srinivas, First and second law analysis for the MHD flow of two immiscible couple stress fluids between two parallel plates, Heat Transfer—Asian Research, 44(5) (2015) 468-487, https://doi.org/10.1002/htj.21131.
13. Raju, Adigoppula, N. Naresh Kumar, and D. R. V. S. R. K. Sastry. Dissipative heat transfer on MHD micropolar hybrid nanofluid flow through infinite parallel squeezing plates. Numerical Heat Transfer, Part B: Fundamentals 86(9) (2025) 3122-3137, https://doi.org/10.1080/10407790.2024.2353793.
14. T. Hayat, R. Sajjad, A. Alsaedi, T. Muhammad, R. Ellahi, On squeezed flow of couple stress nanofluid between two parallel plates, Results in physics, 7 (2017) 553-561, https://doi.org/10.1016/j.rinp.2016.12.038.
15. S. S. Ilani, E. A. Ashmawy, A time dependent slip flow of a couple stress fluid between two parallel plates through state space, J. Taibah University for Science, 12(5) (2018) 592-599, https://doi.org/10.1080/16583655.2018.1510164.

16. A. Raju, O. Ojjela, P. K. Kambhatla, A comparative study of heat transfer analysis on ethylene glycol or engine oil as base fluid with gold nanoparticle in presence of thermal radiation, J. Thermal Analysis and Calorimetry, 145(5) (2021), https://doi.org/10.1007/s10973-020-09757-x.
17. D. Bhargavi, R. Aich, N. Gupta, Thermal enhancement of couple stress fluid flow through anisotropic porous media, Phys. Fluids. 36(4) (2024), https://doi.org/10.1063/5.0200187.
18. R. L. Hamilton, O. K. Crosser, Thermal conductivity of heterogeneous two-component systems, Industrial & Engineering chemistry fundamentals, 1(3) (1962) 187-191. https://doi.org/10.1021/i160003a005.
19. E. V. Timofeeva, J. L. Routbort, D. Singh, Particle shape effects on thermophysical properties of alumina nanofluids, J. app. Phys. 106(1) (2009), https://doi.org/10.1063/1.3155999.
20. I. Khan, Shape effects of MoS2 nanoparticles on MHD slip flow of molybdenum disulphide nanofluid in a porous medium, J. Mole. Liq. 233 (2017) 442-451, https://doi.org/10.1016/j.molliq.2017.03.009.
21. K. Ali Abro, M. Hussain, M. Mahmood Baig, An analytic study of molybdenum disulfide nanofluids using the modern approach of Atangana-Baleanu fractional derivatives. The European Phy. J. Plus, 132(10) (2017), 439, https://doi.org/10.1140/epjp/i2017-11689-y.
22. Preeti, O. Ojjela, P. K. Kambhatla, F. Mebarek-Oudina, Shape effect of MoS 2 nanoparticles on entropy generation and heat transport in viscoelastic boundary layer flow, Pramana, 95(4) (2021) 182, https://doi.org/10.1007/s12043-021-02195-w.
23. S. S. Ghadikolaei, M. Gholinia, 3D mixed convection MHD flow of GO-MoS2 hybrid nanoparticles in H2O–(CH2OH) 2 hybrid base fluid under the effect of H2 bond, Int. Commun. Heat Mass Transfer, 110 (2020) 104371, https://doi.org/10.1016/j.icheatmasstransfer.2019.104371.
24. P. V. Ananth Subray, B. N. Hanumagowda, S. V. K. Varma, M. Hatami, The impacts of shape factor and heat transfer on two-phase flow of nano and hybrid nanofluid in a saturated porous medium, Sci. Rep. 12(1) (2022) 21864, https://doi.org/10.1038/s41598-022-26169-z.
25. S. Li, X. You, Shape-factor impact on a mass-based hybrid nanofluid model for homann stagnation-point flow in porous media, Nanomaterials, 13(6) (2023) 984, https://doi.org/10.3390/nano13060984.

26. A. Ahsan, A. Zanj, A. Zafar, N. Iqbal, A. Fatima, J. Khan, M. W. Guerrero, Predicting the impact of graphene oxide and its shapes on the thermal efficiency of Polyalphaolefin-40 using a mathematical model for wind turbine gearboxes, Case Stud.Ther. Eng. 72 (2025) 106307, https://doi.org/10.1016/j.csite.2025.106307.
27. M. Imran, S. T. Saeed, J. Younis, I. Kebaili, I. Boukhris, A. Mir, ANN-based thermal analysis of 3D MHD hybrid nanofluid flow over a shrinking sheet via LMA, Sci. Rep. 15(1), (2025) 33137, https://doi.org/10.1038/s41598-025-18363-6.
28. M. Arif, L. Di Persio, P. Kumam, W. Watthayu, A. Akgül, Heat transfer analysis of fractional model of couple stress Casson tri-hybrid nanofluid using dissimilar shape nanoparticles in blood with biomedical applications, Sci. Rep. 13(1) (2023) 4596, https://doi.org/10.1038/s41598-022-25127-z.
29. S. Childress, M. Levandowsky, E. A. Spiegel, Pattern formation in a suspension of swimming microorganisms: equations and stability theory, J. Fluid Mech. 69(3) (1975) 591-613, https://doi.org/10.1017/S0022112075001577.
30. B. Bin-Mohsin, N. Ahmed, Adnan, U. Khan, S. Tauseef Mohyud-Din, A bioconvection model for a squeezing flow of nanofluid between parallel plates in the presence of gyrotactic microorganisms, Eur. Phys. J. Plus. 132(4) (2017) 187, https://doi.org/10.1140/epjp/i2017-11454-4.
31. Q. Zhao, H.Xu, L. Tao, Unsteady bioconvection squeezing flow in a horizontal channel with chemical reaction and magnetic field effects, Math. Prob. Eng. 2017(1) (2017) 2541413, https://doi.org/10.1155/2017/2541413.
32. M. D. Shamshuddin, S. R. Mishra, A. Kadir, O. A. Bég, Unsteady chemo-tribological squeezing flow of magnetized bioconvection lubricants: numerical study, J. Nanofluids, 8(2) (2019) 407-419, https://doi.org/10.1166/jon.2019.1587.
33. D. Srinivasacharya, I. Sreenath, Bioconvection in a squeezing flow of a micropolar fluid in a horizontal channel, Heat Transfer Asian Res. 48(6) (2019) 2155-2173, https://doi.org/10.1002/htj.21477.
34. D. Srinivasacharya, I. Sreenath, Unsteady bioconvection in a squeezing flow of a couple-stress fluid through horizontal channel, Int. J. App. Comp. Math. 6(2) (2020) 30, https://doi.org/10.1007/s40819-020-0779-8.
35. A. Raju, O. Ojjela, N. Naresh Kumar, I. Sreenath, Bio-Convective Hartmann Flow of Couple Stress Hybrid Nanofluid Between Two Dilating Parallel Walls with Heat and Mass Transfer, J. Nanofluids, 12(7) (2023) 1794-1803, https://doi.org/10.1166/jon.2023.2053.

36. S. Samal, S. Ontela, Sensitivity analysis and optimization of heat transfer in the time-reliant magnetohydrodynamic bioconvective flow of radiative couple-stress hybrid nanofluid through a squeezing channel with viscous dissipation: entropy analysis, Hybrid Advances, 7 (2024) 100258, https://doi.org/10.1016/j.hybadv.2024.100258.
37. S. Samal, S. Enamul, S. Ontela, Thermal optimization in Hall-induced bioconvective Jeffrey hybrid nanofluid flow in a squeezing channel with activation energy: sensitivity analysis, Chem. Eng. Sci. 318 (2025) 122172, https://doi.org/10.1016/j.ces.2025.122172.
38. E. N. Thabet, A. M. Abd-Alla, H. A. Hosham, S. M. M. El-Kabeir, Entropy generation in peristaltic transport of bio-convective couple stress blood nanofluid with chemotactic microorganisms involving viscous dissipation and slip effects, Alex Eng. J. 102 (2024) 361-380, https://doi.org/10.1016/j.aej.2024.05.062.